Physica E 146 (2023) 115515

Contents lists available at ScienceDirect

Physica E: Low-dimensional Systems and Nanostructures

journal homepage: www.elsevier.com/locate/physe

Waiting time distributions of the electron transport in a quantum dot coupled to a Majorana bound state

Wei Fu [a], Sha-Sha Ke [a,*], Jun-Tong Ren [a], Jun Zhou [a], Hai-Feng Lü [a,b,*]

[a] School of Physics and School of Electronic Science and Engineering, University of Electronic Science and Technology of China, Chengdu 610054, China
[b] Department of Physics and State Key Laboratory of Low-Dimensional Quantum Physics, Tsinghua University, Beijing 100084, China

ARTICLE INFO

Keywords:
Waiting time distribution
Majorana bound state
Topological superconductor

ABSTRACT

We investigate theoretically the waiting time distribution (WTD) of the sub-gap electron transport through a quantum dot which is coupled to two normal metal leads and one Majorana bound state of a topological superconductor. Using the generalized master equation approach, we calculate and present the analytical expressions of the WTDs. It is found that the WTD is an even function of the energy level of the dot. For comparison, we also consider the case that the quantum dot is side coupled to an ordinary fermionic state. For an ordinary fermionic state, the WTD indicates quite different behavior when tuning the dot energy level with opposite signs. Moreover, we discuss the information contained in the $g^{(2)}$ function to investigate the bunching and antibunching of electron tunneling processes.

1. Introduction

Majorana fermion is a fermionic particle which is its own antiparticle [1]. Majorana bound states (MBSs) as the condensed matter realization of majorana fermions have been predicted as the localized quasiparticle excitation in topological superconductors (TSCs) [1]. Topological qubits based on MBSs can store the quantum information nonlocally, which make them promising building blocks for topological quantum computation [2–6]. The experimental signals of MBSs, especially the local charge tunneling measurement of the zero-bias conductance peaks (ZBCPs), have been reported [7–15] in several leading candidate condensed matter systems, such as superconductor–semiconductor nanowire heterostructure. In the tunneling spectroscopy, the MBSs result in ZBCPs of the quantized value $2e^2/h$. Although the ZBCPs observed in the early experiments in 2012 are consistent with MBSs, the small value of ZBCPs and alternative explanations with non-topological origin made the existence of MBSs inconclusive [16–21]. With the development of device fabrication, more recently, experiments have observed the large ZBCPs with value $\sim 2e^2/h$ in the nanowire hybrid system [22,23]. However, as an evidence for nonlocality of the MBSs, the ZBCPs have never been simultaneously detected at the two ends of a nanowire [22]. Moreover, it has been showed that very high amount of disorder in the nanowire could give rise to these large ZBCPs [22,24]. Due to the lack of conclusive evidence, the existence of MBSs in condensed matter system remains controversial.

To describe quantum statistical properties of charge transfers in mesoscopic devices, the full counting statistics (FCS) [25,26] has widely been used, and it provides complete statistical information about the low-frequency fluctuations of the number of transferred charges. Differently, the waiting time distribution (WTD) has been proven to be a useful tool to capture the information about short-time physics [27]. The WTD represents the distribution of the time interval between two successive electron transmissions [28–32]. It can reveal interesting short-time physics that is inaccessible in long-time FCS [27,33]. Spurred by the rapid development of real-time single electron detection techniques [34], experimental measurement of microscopic current fluctuations and waiting times between interval tunneling events have been realized in various quantum devices [35,36]. Recently, the real-time observation of splitting of individual Cooper pairs has been realized, enabling direct access to the time-resolved statistics of Cooper pair splitting. The correlation statistics extracted from two-electron processes indicates a pronounced peak that is two orders of magnitude larger than the background, implying the highly-efficient splitting of Cooper pairs [37]. The results open up a new avenue for detecting the dynamical tunneling processes and probing the inner dynamics in mesoscopic devices.

Closely related to the recent experiments on WTDs, it is highly desirable to discriminate Majorana bound states from other trivial states by short-time correlation properties between successive electron

* Corresponding author at: School of Physics and School of Electronic Science and Engineering, University of Electronic Science and Technology of China, Chengdu 610054, China.
E-mail addresses: keshasha@uestc.edu.cn (S.-S. Ke), lvhf04@uestc.edu.cn (H.-F. Lü).

https://doi.org/10.1016/j.physe.2022.115515
Received 18 April 2022; Received in revised form 16 September 2022; Accepted 27 September 2022
Available online 14 October 2022

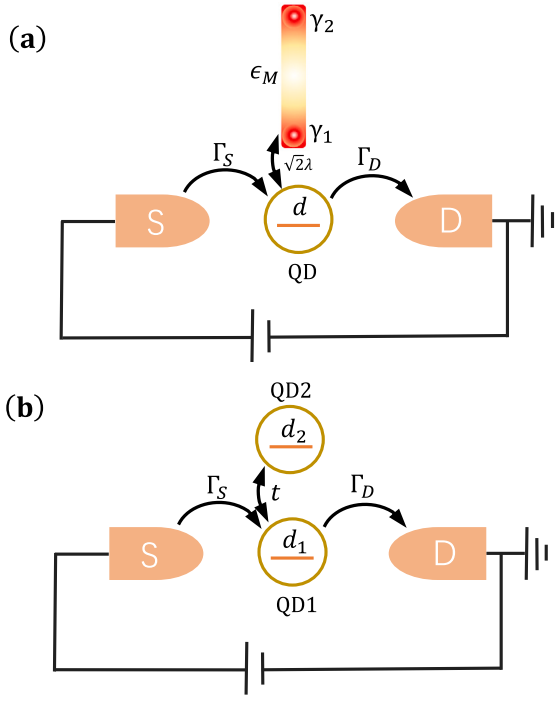

Fig. 1. Schematic setup: (a) a single-level quantum dot coupled one MBS localized at the one end of the TSC nanowire is connected to metallic source and drain electrodes (dot-MBS system). The wave functions of MBSs localized at two ends hybridize and induce a finite Majorana splitting ϵ_M. (b) The setup with the MBS being replaced by a side-coupled ordinary fermionic state (dot–dot system).

tunneling events. Up to now, the study on WTDs for electron transport through a quantum-dot system coupled to MBSs is still missing. In this paper, we consider WTDs of the electron transport through a quantum dot side-coupled to a MBS hosted in a topological superconductor. The paper is organized as follows. In Section 2, we introduce the model Hamiltonian of the considered setup, as well as the formulas for calculating the WTD and other statistics. We also consider the case that the quantum dot is side-coupled to an ordinary fermionic mode. In Section 3, we investigate the WTD related properties modulated by dot energy level and the Majorana energy splitting. Finally, a summary is given in Section 4.

2. Model and formula

We consider the setup shown in Fig. 1(a) in which a single-level quantum dot is coupled to a MBS γ_1 localized at one end of a TSC nanowire. The electron on the quantum dot is tunneling coupled to non-interacting electrons in two metallic leads acting as the source and drain. In the following we assume that Coulomb interactions are strong enough to prevent more than one electron on the quantum dot. The effective low-energy Hamiltonian of this dot-MBS system with a large superconducting gap is given by [38–40]

$$H_{\rm eff} = \epsilon_D d^\dagger d + i\epsilon_M \gamma_1\gamma_2 + \sqrt{2}\lambda(d^\dagger - d)\gamma_1, \tag{1}$$

where $d^\dagger$ creates an electron with energy ϵ_D in the single-level quantum dot, ϵ_M is the Majorana splitting energy due to the overlap of two MBSs, $\sqrt{2}\lambda$ denotes the coupling strength between the dot and the MBS γ_1. By expressing two Majorana operators in terms of a non-local fermion f as $\gamma_1 = (f^\dagger + f)/\sqrt{2}$ and $\gamma_2 = i(f^\dagger - f)/\sqrt{2}$, we can rewrite the dot-MBS Hamiltonian as [41,42]

$$H_{\rm eff} = \epsilon_D d^\dagger d + \epsilon_M (f^\dagger f - \frac{1}{2}) + \left[\lambda(d^\dagger f^\dagger + d^\dagger f) + \text{H.c.}\right]. \tag{2}$$

The leads are modeled as reservoirs of noninteracting spinless fermions and described by

$$H_{\rm leads} = \sum_{\alpha=S,D}\sum_k \epsilon_{\alpha k} c^\dagger_{\alpha k} c_{\alpha k}. \tag{3}$$

Here, $c^\dagger_{\alpha k}$ is the electron creation operator with momentum k and energy $\epsilon_{\alpha k}$ in the lead α. The Hamiltonian for electron tunneling processes between two leads and the quantum dot takes the form

$$H_{\rm tunn} = \sum_{\alpha=S,D}\sum_k V_\alpha c^\dagger_{\alpha k} d + \text{H.c.}, \tag{4}$$

where V_α is the momentum-independent tunneling matrix element.

Since we are interested in the WTD for unidirectional electron transport in subgap regime, we employ the Markovian generalized master equation for the density operator in the large bias limit, which takes into account the quantum coherent processes. In Liouville space, the time evolution of system density matrix can be written as [43]

$$\dot\rho = \mathcal{W}\rho = -i[H_{\rm eff}, \rho] + \mathcal{D}[\rho], \tag{5}$$

where $\mathcal{D}[\rho]$ is the Lindblad dissipator, $\mathcal{W}$ is called the Liouvillian, and we set $\hbar = 1$. After introducing the counting field χ to count the electrons tunneling into the drain from the dot, we get the dissipator [44]:

$$\mathcal{D}[\rho] = \Gamma_D(e^{-i\chi} d\rho d^\dagger - \frac{1}{2}\{\rho, d^\dagger d\}) + \Gamma_S(d^\dagger \rho d - \frac{1}{2}\{\rho, d d^\dagger\}), \tag{6}$$

where $\Gamma_\alpha = 2\pi\sum_k |V_\alpha|^2\delta(\omega - \epsilon_{\alpha k})$ is the coupling strength between lead α and the dot in the wide-band limit.

To write down the explicit matrix form of the Liouvillian, we choose the empty-dot state $|0\rangle$, the singly occupied dot state $|d/f\rangle = d^\dagger/f^\dagger|0\rangle$, and the double-occupied state $|D\rangle = d^\dagger f^\dagger|0\rangle$ as the basis. Then, the relevant entries of density matrix form the basis in Liouville space $\{\rho_{00}, \rho_{dd}, \rho_{ff}, \rho_{DD}, \rho_{df}, \rho_{fd}, \rho_{D0}, \rho_{0D}\}$, where $\rho_{ij} = \langle i|\rho|j\rangle$ with $|i/j\rangle \in \{|0\rangle, |d\rangle, |f\rangle, |D\rangle\}$. Finally, the Liouvillian in this basis reads Eq. (7) (see Box I) where $\Gamma_0 = (\Gamma_S + \Gamma_D)/2$, $\delta = \epsilon_D - \epsilon_M$ is the detuning between two singly occupied dot states, $\epsilon = \epsilon_M + \epsilon_D$ is the energy difference between empty state and double-occupied state.

Due to the statistical nature of the density matrix, the time elapse τ between two subsequent electron jumps is not a constant value. Instead, it is described by a probability distribution, i.e., the waiting time distribution. To formulate the WTDs, we rewrite the Liouvillian $\mathcal{W}(\chi)$ as

$$\mathcal{W}(\chi) = \mathcal{W}_0 + \mathcal{J}e^{-i\chi}, \tag{8}$$

where $\mathcal{W}_0$ generates the time evolution of ρ with no electron jumping from lead to the dot-MBS system, and $\mathcal{J}$ describes a electron tunneling event from the dot into the drain electrode. The distribution of electron waiting time is defined as [45]

$$w(\tau) = \frac{\text{Tr}[\mathcal{J}e^{\mathcal{W}_0\tau}\mathcal{J}\rho_S]}{\text{Tr}[\mathcal{J}\rho_S]}, \tag{9}$$

where the system is initially in the stationary state ρ_S. The stationary state limit $\lim_{\tau\to\infty}\rho(\tau) = \rho_S$ leads to the stationary state ρ_S satisfying $\mathcal{W}(0)\rho_S = 0$. Instead of directly calculating the WTD with the expression given by Eq. (9), it may be more convenient to first evaluate the Laplace transform of the WTD

$$\hat w(z) = \int_0^\infty d\tau e^{-z\tau} w(\tau) = \frac{\text{Tr}[\mathcal{J}(z - \mathcal{W}_0)^{-1}\mathcal{J}\rho_S]}{\text{Tr}[\mathcal{J}\rho_S]}. \tag{10}$$

The WTD then can be obtained by performing inverse Laplace transform.

To better understand the statistical properties of electron waiting time, it is also instructive to study the $g^{(2)}$ function which has been used to identify the bunching and antibunching in electron transport. Using master-equation formalism, the $g^{(2)}$ function can be defined as [46]

$$g^{(2)}(\tau) = \frac{\text{Tr}[\mathcal{J}e^{\mathcal{W}(0)\tau}\mathcal{J}\rho_S]}{\text{Tr}[\mathcal{J}\rho_S]^2}. \tag{11}$$

$$\mathcal{W}(\chi)=\begin{pmatrix} -\Gamma_S & \Gamma_D e^{-i\chi} & 0 & 0 & 0 & 0 & i\lambda & -i\lambda \\ \Gamma_S & -\Gamma_D & 0 & 0 & i\lambda & -i\lambda & 0 & 0 \\ 0 & 0 & -\Gamma_S & \Gamma_D e^{-i\chi} & -i\lambda & i\lambda & 0 & 0 \\ 0 & 0 & \Gamma_S & -\Gamma_D & 0 & 0 & -i\lambda & i\lambda \\ 0 & i\lambda & -i\lambda & 0 & i\delta-\Gamma_0 & 0 & 0 & 0 \\ 0 & -i\lambda & i\lambda & 0 & 0 & -i\delta-\Gamma_0 & 0 & 0 \\ i\lambda & 0 & 0 & -i\lambda & 0 & 0 & i\epsilon-\Gamma_0 & 0 \\ -i\lambda & 0 & 0 & i\lambda & 0 & 0 & 0 & -i\epsilon-\Gamma_0 \end{pmatrix}, \tag{7}$$

Box I.

The $g^{(2)}$ function gives the conditional probability that an electron is tunneled into the drain at time $\tau = 0$, and a successive electron jump occurs at time τ[47].

Another interesting quantity is the Pearson correlation coefficient which is given by [48]

$$P=\frac{\langle\tau\tau'\rangle-\langle\tau\rangle^2}{\langle\langle\tau^2\rangle\rangle}, \tag{12}$$

where $\langle\tau\rangle$ is the average waiting time, $\langle\langle\tau^2\rangle\rangle = \langle\tau^2\rangle - \langle\tau\rangle^2$ is the variance and $\langle\tau\tau'\rangle$ is the first moment of the joint probability distribution [48]

$$w_2(\tau,\tau')=\frac{\mathrm{Tr}[\mathcal{J}e^{\mathcal{W}_0\tau'}\mathcal{J}e^{\mathcal{W}_0\tau}\mathcal{J}\rho_S]}{\mathrm{Tr}[\mathcal{J}\rho_S]}. \tag{13}$$

Here, the $w_2(\tau,\tau')$ describes the probability density that, given an initial electron tunneling, it takes time τ' for the next tunneling and τ' for another tunneling after that. The Pearson correlation coefficient characterizes the correlation between two successive waiting times τ and τ'.

As a comparison, we also examine the time-resolved statistics in a quantum dot side-coupled to an ordinary fermionic state of another dot. As the setup shown in Fig. 1(b), the dot 1 is coupled to two metal leads, and the Hamiltonian of this dot–dot system reads

$$H_{\mathrm{eff}}=\epsilon_{D1}d_1^\dagger d_1+\epsilon_{D2}d_2^\dagger d_2+t(d_1^\dagger d_2+d_2^\dagger d_1), \tag{14}$$

where ϵ_{D1} and ϵ_{D2} represent dot energy level of the dot 1 and dot 2, respectively, t denotes the interdot coupling. The quantum transport through this device has been widely discussed in several previous literatures [49–51]. Especially, the super-Poissonian shot noise could be induced for a relatively small interdot coupling t. Compared with the case of coupled to a MBS, there is no pairing term between two fermionic states. When the dot is coupled to a MBS, the system holds the particle-hole symmetry under the transformation of $\epsilon_D \to -\epsilon_D$ and $d \to d^\dagger$. Therefore, the WTD is expected to be symmetric about $\epsilon_D = 0$ when tuning the dot energy levels. While for the case of quantum dot side-coupled to an ordinary fermionic state, the WTD becomes asymmetric and depends on the energy level ϵ_{D2} of the coupled dot 2.

3. Results and discussions

To perform the calculations, we choose to evaluate the WTDs in the Laplace space. For the symmetric coupling strength $\Gamma_S = \Gamma_D = \Gamma$, we find the analytical expression of the WTD $\hat{w}_{\mathrm{MBS}}(z)$ for a dot-MBS system:

$$\hat{w}_{\mathrm{MBS}}(z)=\frac{\Gamma\left[\lambda^2(2\Gamma+z)^2A+\Gamma(\Gamma+z)B+4\lambda^4C\right]}{(\Gamma+z)^3\left(4\lambda^2A+B\right)+4\lambda^4(\Gamma+2z)C}, \tag{15}$$

where $A=\delta^2+\epsilon^2+2(\Gamma+z)^2$, $B=(\delta^2+(\Gamma+z)^2)(\epsilon^2+(\Gamma+z)^2)$, and $C=(\Gamma+z)(3\Gamma+2z)$. The exact expression for the Liouvillian of the dot–dot system is given in the appendix, and the corresponding $\hat{w}_{\mathrm{dot}}(z)$ reads

$$\hat{w}_{\mathrm{dot}}(z)=\frac{\Gamma\left[\Gamma(\Gamma+z)\left(\tilde{\delta}^2+(\Gamma+z)^2\right)+t^2(2\Gamma+z)^2\right]}{(\Gamma+z)^3\left(\tilde{\delta}^2+4t^2+(\Gamma+z)^2\right)} \tag{16}$$

with $\tilde{\delta}=\epsilon_{D1}-\epsilon_{D2}$ being the detuning between the occupied sates in each dot. The WTDs can be obtained by performing the inverse Laplace transform of Eqs. (15) and (16).

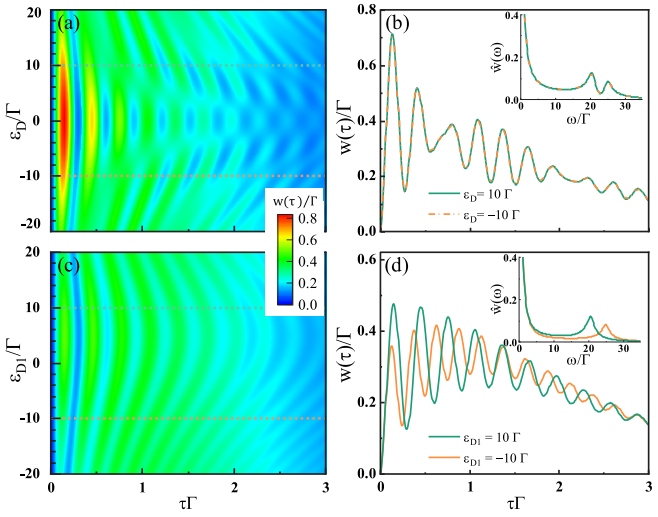

Fig. 2. (a) Distributions of electron waiting time as a function of the dot energy level ϵ_D in dot-MBS system with $\epsilon_M = 5\Gamma$. (b) WTDs along the dotted line-cuts indicated in the panel (a). (c) Distributions of electron waiting time as a function of the dot energy level ϵ_{D1} in dot–dot system with $\epsilon_{D2} = 5\Gamma$. (d) WTDs along the dotted line-cuts indicated in the left panel (c). Other parameters are $\Gamma_{S/D} = \Gamma$ and $\lambda = t = 10\Gamma$.

For the fixed value of ϵ_M and ϵ_{D2}, we choose different energies ϵ_D and ϵ_{D1} of the dot level and present the results of WTDs in Fig. 2. In both setups, right after an electron tunneling to the drain, the dot coupled directly to the drain is empty. The subsequent electron has to first refill the dot before it could tunnel into the drain. Therefore, two electrons cannot simultaneously tunnel to the drain and the WTDs are zero at $\tau = 0$, as shown in Fig. 2(b) and (d). We notice that, for the dot level with energy $\pm\epsilon_D$, the WTDs show same behaviors in the dot-MBS system, while the corresponding WTDs are significantly different in a dot–dot system. From the expression Eq. (15), we see that $\hat{w}_{\mathrm{MBS}}(z)$ is a function of δ and ϵ, and remains unchanged when exchanging the values of δ and ϵ. Consequently, the WTD is an even function of the Majorana energy splitting and the energy of the dot level. However, $\hat{w}_{\mathrm{dot}}(z)$ in Eq. (16) depends only on the magnitude of $\tilde{\delta}$, leading to different WTDs for $\pm\epsilon_{D1}$ when ϵ_{D2} is non-vanishing. As the detuning $\tilde{\delta}$ between two singly occupied states increases, the

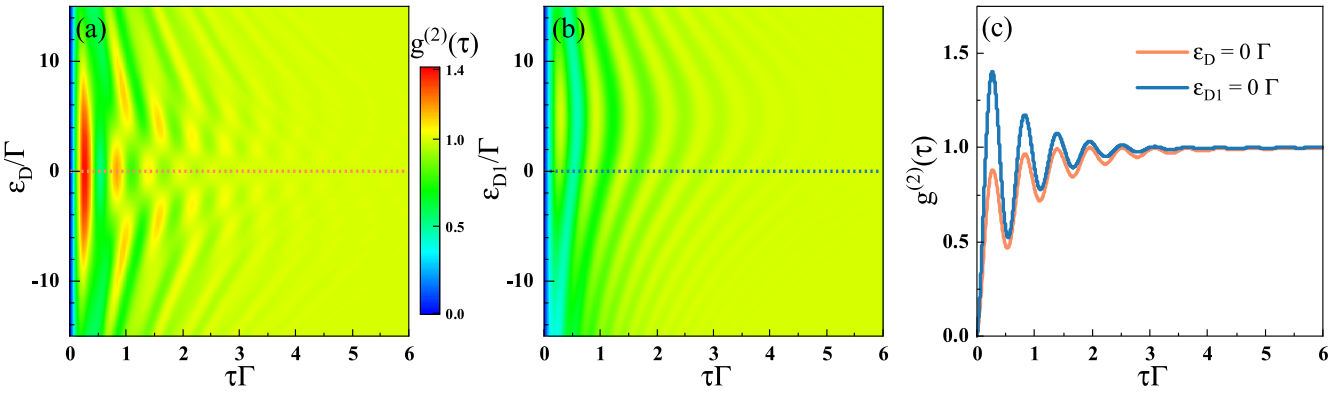

Fig. 3. (a) The $g^{(2)}$ function as a function of the dot energy level ϵ_D in dot-MBSs system with $\epsilon_M = 5\Gamma$. (b) The $g^{(2)}$ function as a function of the energy level ϵ_{D1} in dot–dot system with $\epsilon_{D2} = 5\Gamma$. (c) The $g^{(2)}(\tau)$ along the dotted line-cuts indicated in the panel (a) and (b). Other parameters are $\Gamma_{S/D} = \Gamma$ and $\lambda = t = 5\Gamma$.

amplitude of the oscillation is reduced and its frequency is increased. It is also important to emphasize that the WTDs are oscillatory. The oscillations are originated from the quantum coherence between two states in the even or odd occupation sector [43]. Furthermore, the oscillation frequencies can be revealed in the Fourier transform of the WTD, which is explicitly given by

$$\hat{w}(\omega) = \frac{\mathrm{Tr}[\mathcal{J}(i\omega\mathbf{I} - \mathcal{W}_0)^{-1}\mathcal{J}\rho_S]}{\mathrm{Tr}[\mathcal{J}\rho_S]}. \tag{17}$$

On the other hand, the eigenstates of the dot-MBS system can be easily obtained by diagonalizing the Hamiltonian Eq. (2) and read

$$|o,\pm\rangle = \frac{1}{\sqrt{2}}\sqrt{1 \mp \delta/\epsilon_1}|d\rangle \mp \frac{1}{\sqrt{2}}\sqrt{1 \pm \delta/\epsilon_1}|f\rangle, \tag{18}$$

$$|e,\pm\rangle = \frac{1}{\sqrt{2}}\sqrt{1 \mp \delta/\epsilon_2}|0\rangle \mp \frac{1}{\sqrt{2}}\sqrt{1 \pm \delta/\epsilon_2}|D\rangle, \tag{19}$$

where $\epsilon_1 = \sqrt{\delta^2 + 4\lambda^2}$ and $\epsilon_2 = \sqrt{\epsilon^2 + 4\lambda^2}$. And the respective eigenvalues are

$$E_{|o,\pm\rangle} = \frac{\epsilon_D}{2} \pm \frac{\epsilon_1}{2}, \qquad E_{|e,\pm\rangle} = \frac{\epsilon_D}{2} \pm \frac{\epsilon_2}{2}. \tag{20}$$

In the case of the dot-MBS system, there are two peaks at the frequencies $\omega_o = \epsilon_1$ and $\omega_e = \epsilon_2$, as shown in the inset in Fig. 2(b). Similarly, for the dot–dot system, we find that a single peak at $\omega = \sqrt{\tilde{\delta}^2 + 4t^2}$ [see the inset in Fig. 2(d)].

Note that the two systems considered here are not single-reset system, and there is no simple relation between the $g^{(2)}$ function and the WTD [46]. The $g^{(2)}$ functions is supposed to reveal additional information about the electron transport statistics. In the Laplace space, analytically, we obtain

$$\hat{g}^{(2)}_{\mathrm{MBS}}(z) = \frac{2\lambda^2(\Gamma + z)[(A+4)(\Gamma + z) + A\Gamma] + 2B\Gamma z}{4\lambda^2 z\left(A + 4\lambda^2\right)(\Gamma + z)^2 + Bz^2(2\Gamma + z)}, \tag{21}$$

for the dot-MBS system and

$$\hat{g}^{(2)}_{\mathrm{dot}}(z) = \frac{2\Gamma z\left(\delta^2 + (\Gamma + z)^2\right) + 2t^2(\Gamma + z)(2\Gamma + z)}{z\left(z(2\Gamma + z)\left(\delta^2 + (\Gamma + z)^2\right) + 4t^2(\Gamma + z)^2\right)}, \tag{22}$$

for the dot–dot system. In Fig. 3, we present the numerical results of the $g^{(2)}$ functions as a function of ϵ_D and ϵ_{D1}, respectively. In both cases, the source and drain are tunneling coupled to a single-level quantum, giving rise to $g^{(2)}(0) = 0$ [46], as shown in Fig. 3(c). Since $g^{(2)}(\tau)$ is always positive, we have $g^{(2)}(\tau) > g^{(2)}(0)$, which indicates that electron emission from the quantum dot is antibunched [46]. Here, the coherent tunneling processes are reflected in the damped oscillatory pattern. As depicted in Fig. 3(a) and (b), the $g^{(2)}$ function of the dot-MBS system is still an even function of the dot energy level, and the oscillation amplitude of the $g^{(2)}$ function is significantly enlarged. Importantly, we find that the value of the $g^{(2)}$ function in the dot–dot system never exceed one, while the $g^{(2)}$ function in a dot-MBS system can be larger than one. In fact, this feature is general and independent of the other parameters of the system. For the dot–dot system, the interdot hopping has two effects. On the one hand, the interdot hopping introduces the quantum coherence in the tunneling processes which allows an electron travel back and forth between two dots before entering into the drain. On the other hand, it also opens another tunneling channel formed by the doubly occupied state and the singly occupied state in the side dot. In this case, the system resembles a quantum dot model consisting of an empty state, a spin-up level and a spin-down level. Obviously, there is no dynamical channel blockade [52] because both channels are generated by the same ordinary fermionic mode coupled to two leads. In the absence of quantum coherence, the $g^{(2)}$ function in this quantum dot system takes the form [46]

$$g^{(2)}(\tau) = 1 - e^{-(2\Gamma_S + \Gamma_D)\tau}, \tag{23}$$

which is different from that of a single-resonant-level model [46]. In the dot–dot system, quantum coherence imprints oscillation on the $g^{(2)}$ function, but it remains to takes value smaller than one. Differently, in the dot-MBS system, the coupling between the dot level and the MBS also results in quantum coherence in the even occupation sector. Here, we may assume that $|D\rangle$ and $|f\rangle$ form a single level system, while the $|0\rangle$ and $|d\rangle$ establish the other single-level system. Due to the internal dynamics of the dot-MBS system, an electron is allowed to oscillate back and form between two single level system. Therefore, the dot-MBS system behaves more like a serial double quantum dot. Its $g^{(2)}$ function, as shown in Fig. 3(c), is similar to that of a serial double quantum dot [29,46].

Finally, we calculate the Pearson correlation coefficient as a function of two energy levels for two systems, respectively. The results are presented in Fig. 4. In mesoscopic electron transport, the renewal assumption for the WTD is given by [48]

$$w_2(\tau, \tau') = w(\tau)w(\tau'). \tag{24}$$

If the renewal assumption is justified, by definition, the Pearson correlation coefficient is zero, and there is no temporal correlations between two successive waiting times. As we can see from Fig. 4, for both systems, the Pearson correlation coefficient is negative, implying that the electron transport is a non-renewal process. On the other hand, negative correlations indicate that a longer (shorter) than average τ is likely to be followed by a shorter (longer) than average τ'. This temporal feature is consistent with the our previous conclusion that electron transport is antibunched through the analysis of $g^{(2)}$ function. In Fig. 4(a), we also notice that the negative correlation in the dot-MBS system are strongly suppressed when $\epsilon_D = 0$ or $\epsilon_M = 0$. For the dot–dot system, we find that the negative correlation is strongly enhanced along the axis $\epsilon_{D1} = \epsilon_{D2}$. Such properties can hardly be revealed in the WTDs and $g^{(2)}$ function.

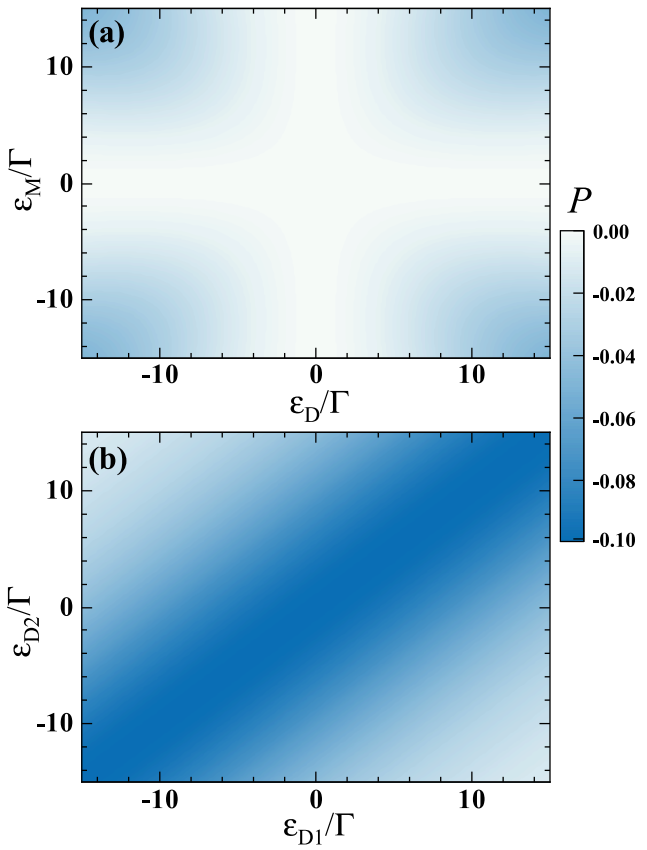

Fig. 4. (a) The Pearson correlation coefficient of the dot-MBS system as a function of ϵ_M and ϵ_D. (c) The Pearson correlation coefficient of the dot–dot system as a function of ϵ_{D1} and ϵ_{D2}. Other parameter are the same as that of Fig. 2.

4. Conclusion

In this work we have explored the time-resolved statistics for the electron transport through a quantum dot which is coupled to two normal metal leads and one MBS or an ordinary fermionic state, respectively. Using generalized master equation approach, we evaluated the electron WTD, the $g^{(2)}$ function as well as the Pearson correlation coefficient. Based the analytical expressions of the WTDs and the $g^{(2)}$ function, we have presented the detailed analysis of internal dynamics of both systems. Most importantly, it is observed that both the WTD and $g^{(2)}$ function are an even function of two energy levels for the dot-MBS system. While, for the dot–dot system, such a property does not exist, and the $g^{(2)}$ function is always smaller than one. In both systems, the $g^{(2)}$ function indicated that electron emission from the dot is antibunched, which is consistent with the results of Pearson correlation coefficient.

Natural extensions of the present study of the WTD in dot-MBS system include considering the WTDs with Coulomb interaction on the TSC nanowire and more refined tunneling Hamiltonian [53], as well as how the WTDs at finite bias voltage can manifest interaction effects in quantum dot system with MBSs [54]. Recent experiments have realized the real-time detection of single electron in quantum dots and the direct access the WTDs and $g^{(2)}$ function [37]. Experimentally, the energy level in a quantum dot is tunable via a gate voltage. We expect that some features in the time-resolved statistics stemming from the presence of MBSs may be utilized for the identification of MBSs in a mesoscopic device.

Declaration of competing interest

The authors declare that they have no known competing financial interests or personal relationships that could have appeared to influence the work reported in this paper.

Data availability

Data will be made available on request.

Acknowledgments

This work was supported by the Natural Science Foundation of China (Grant No. 12074209, No. 12274063), the Fundamental Research Funds for the Central Universities, China (Grant No. ZYGX2019J100), and the Open Project of the State Key Laboratory of Low-Dimensional Quantum Physics, China (Grant No. KF202008).

Appendix. The Liouvillian of the dot–dot system

In the localized dot basis $\{|0\rangle, |d_1\rangle, |d_2\rangle, |D\rangle\}$ with $|d_i\rangle = d_i^\dagger|0\rangle$ $(i = 1, 2)$ and $|D\rangle = d_1^\dagger d_2^\dagger|0\rangle$, we have basis $\left\{\rho_{00}, \rho_{d_1d_1}, \rho_{d_2d_2}, \rho_{DD}, \rho_{d_1d_2}, \rho_{d_2d_1}\right\}$ for Liouville space. The Liouvillian with the counting field χ can be obtained as

$$\mathcal{W}(\chi) = \begin{pmatrix} -\Gamma_S & \Gamma_D e^{-i\chi} & 0 & 0 & 0 & 0 \\ \Gamma_S & -\Gamma_D & 0 & 0 & it & -it \\ 0 & 0 & -\Gamma_S & \Gamma_D e^{-i\chi} & -it & it \\ 0 & 0 & \Gamma_S & -\Gamma_D & 0 & 0 \\ 0 & it & -it & 0 & -i\tilde{\delta} - \Gamma_0 & 0 \\ 0 & -it & it & 0 & 0 & i\tilde{\delta} - \Gamma_0 \end{pmatrix}, \quad \text{(A.1)}$$

where $\Gamma_0 = (\Gamma_S + \Gamma_D)/2$. From Eq. (A.1), one can readily read off the jump superoperator $\mathcal{J}$.

References

[1] J. Alicea, New directions in the pursuit of majorana fermions in solid state systems, Rep. Progr. Phys. 75 (7) (2012) 076501, http://dx.doi.org/10.1088/0034-4885/75/7/076501.

[2] C. Nayak, S.H. Simon, A. Stern, M. Freedman, S. Das Sarma, Non-abelian anyons and topological quantum computation, Rev. Modern Phys. 80 (2008) 1083–1159, http://dx.doi.org/10.1103/RevModPhys.80.1083, URL https://link.aps.org/doi/10.1103/RevModPhys.80.1083.

[3] S.D. Sarma, M. Freedman, C. Nayak, Majorana zero modes and topological quantum computation, NPJ Quant. Inf. 1 (2015) 15001, http://dx.doi.org/10.1038/npjqi.2015.1.

[4] D. Aasen, M. Hell, R.V. Mishmash, A. Higginbotham, J. Danon, M. Leijnse, T.S. Jespersen, J.A. Folk, C.M. Marcus, K. Flensberg, J. Alicea, Milestones toward majorana-based quantum computing, Phys. Rev. X 6 (2016) 031016, http://dx.doi.org/10.1103/PhysRevX.6.031016, URL https://link.aps.org/doi/10.1103/PhysRevX.6.031016.

[5] M. Bharati, V. Soma, Flexible SERS substrates for hazardous materials detection: recent advances, Opto-Electron. Adv. 4 (11) (2021) 210048, http://dx.doi.org/10.29026/oea.2021.210048, URL https://www.oejournal.org/article/doi/10.29026/oea.2021.210048.

[6] Y. Hu, D. Liang, R. Beausoleil, An advanced III-V-on-silicon photonic integration platform, Opto-Electron. Adv. 4 (9) (2021) 200094, http://dx.doi.org/10.29026/oea.2021.200094, URL https://www.oejournal.org/article/doi/10.29026/oea.2021.200094.

[7] V. Mourik, K. Zuo, S.M. Frolov, S.R. Plissard, E. Bakkers, L.P. Kouwenhoven, Signatures of majorana fermions in hybrid superconductor-semiconductor nanowire devices, Science 336 (2012) 1003–1007, http://dx.doi.org/10.1126/science.1222360, URL http://www-science-org-s.vpn.uestc.edu.cn:8118/doi/10.1126/science.1222360.

[8] M.T. Deng, S. Vaitiekėnas, E.B. Hansen, J. Danon, M. Leijnse, K. Flensberg, J. Nygård, P. Krogstrup, C.M. Marcus, Majorana bound state in a coupled quantum-dot hybrid-nanowire system, Science 354 (6319) (2016) 1557–1562, http://dx.doi.org/10.1126/science.aaf3961.

[9] S.M. Albrecht, A.P. Higginbotham, M. Madsen, F. Kuemmeth, T.S. Jespersen, J. Nygård, P. JKrogstrup, C.M. Marcus, Exponential protection of zero modes in majorana islands, Nature 531 (2016) 206–209, http://dx.doi.org/10.1038/nature17162.

[10] X. Zhao, W. Deng, Printing photovoltaics by electrospray, Opto-Electron. Adv. 3 (6) (2020) 190038, http://dx.doi.org/10.29026/oea.2020.190038, URL https://www.oejournal.org/article/doi/10.29026/oea.2020.190038.

[11] S. Nadj-Perge, I.K. Drozdov, J. Li, H. Chen, S. Jeon, J. Seo, A.H. MacDonald, B.A. Bernevig, A. Yazdani, Observation of majorana fermions in ferromagnetic atomic chains on a superconductor, Science 346 (6209) (2014) 602–607, http://dx.doi.org/10.1126/science.1259327.

[12] A. Sharbirin, S. Akhtar, J. Kim, Light-emitting mxene quantum dots, Opto-Electron. Adv. 4 (3) (2021) 200077, http://dx.doi.org/10.29026/oea.2021.200077, URL https://www.oejournal.org/article/doi/10.29026/oea.2021.200077.

[13] P. Fan, F. Yang, G. Qian, H. Chen, Y.-Y. Zhang, G. Li, Z. Huang, Y. Xing, L. Kong, W. Liu, K. Jiang, C. Shen, S. Du, J. Schneeloch, R. Zhong, G. Gu, Z. Wang, H. Ding, H.-J. Gao, Observation of magnetic adatom-induced majorana vortex and its hybridization with field-induced majorana vortex in an iron-based superconductor, Nature Commun. 12 (2021) 1348, http://dx.doi.org/10.1038/s41467-021-21646-x.

[14] Z. Wan, X. Chen, M. Gu, Laser scribed graphene for supercapacitors, Opto-Electron. Adv. 4 (7) (2021) 200079, http://dx.doi.org/10.29026/oea.2021.200079, URL https://www.oejournal.org/article/doi/10.29026/oea.2021.200079.

[15] J.-T. Ren, S.-S. Ke, Y. Guo, H.-W. Zhang, H.-F. Lü, Phase diagram and quantum transport in a semiconductor-superconductor hybrid nanowire with long-range pairing interactions, Phys. Rev. B 103 (2021) 045428, http://dx.doi.org/10.1103/PhysRevB.103.045428, URL https://link.aps.org/doi/10.1103/PhysRevB.103.045428.

[16] J. Liu, A.C. Potter, K.T. Law, P.A. Lee, Zero-bias peaks in the tunneling conductance of spin-orbit-coupled superconducting wires with and without majorana end-states, Phys. Rev. Lett. 109 (2012) 267002, http://dx.doi.org/10.1103/PhysRevLett.109.267002, URL https://link.aps.org/doi/10.1103/PhysRevLett.109.267002.

[17] H.J. Suominen, M. Kjaergaard, A.R. Hamilton, J. Shabani, C.J. Palmstrøm, C.M. Marcus, F. Nichele, Zero-energy modes from coalescing andreev states in a two-dimensional semiconductor-superconductor hybrid platform, Phys. Rev. Lett. 119 (2017) 176805, http://dx.doi.org/10.1103/PhysRevLett.119.176805, URL https://link.aps.org/doi/10.1103/PhysRevLett.119.176805.

[18] C. Moore, C. Zeng, T.D. Stanescu, S. Tewari, Quantized zero-bias conductance plateau in semiconductor-superconductor heterostructures without topological majorana zero modes, Phys. Rev. B 98 (2018) 155314, http://dx.doi.org/10.1103/PhysRevB.98.155314, URL https://link.aps.org/doi/10.1103/PhysRevB.98.155314.

[19] J. Chen, B.D. Woods, P. Yu, M. Hocevar, D. Car, S.R. Plissard, E.P.A.M. Bakkers, T.D. Stanescu, S.M. Frolov, Ubiquitous non-majorana zero-bias conductance peaks in nanowire devices, Phys. Rev. Lett. 123 (2019) 107703, http://dx.doi.org/10.1103/PhysRevLett.123.107703, URL https://link.aps.org/doi/10.1103/PhysRevLett.123.107703.

[20] A. Vuik, B. Nijholt, A.R. Akhmerov, M. Wimmer, Reproducing topological properties with quasi-majorana states, SciPost Phys. 7 (2019) 61, http://dx.doi.org/10.21468/SciPostPhys.7.5.061, URL https://scipost.org/10.21468/SciPostPhys.7.5.061.

[21] C. Jünger, R. Delagrange, D. Chevallier, S. Lehmann, K.A. Dick, C. Thelander, J. Klinovaja, D. Loss, A. Baumgartner, C. Schönenberger, Magnetic-field-independent subgap states in hybrid rashba nanowires, Phys. Rev. Lett. 125 (2020) 017701, http://dx.doi.org/10.1103/PhysRevLett.125.017701, URL https://link.aps.org/doi/10.1103/PhysRevLett.125.017701.

[22] P. Yu, J. Chen, M. Gomanko, G. Badawy, E.P.A.M. Bakkers, K. Zuo, V. Mourik, S.M. Frolov, Non-majorana states yield nearly quantized conductance in proximatized nanowires, Nat. Phys. 17 (2021) 482–488, http://dx.doi.org/10.1038/s41567-020-01107-w.

[23] D. Pan, H. Song, S. Zhang, L. Liu, L. Wen, D. Liao, R. Zhuo, Z. Wang, Z. Zhang, S. Yang, J. Ying, W. Miao, R. Shang, H. Zhang, J. Zhao, *In situ* epitaxy of pure phase ultra-thin inas-al nanowires for quantum devices, Chin. Phys. Lett. 39 (5) (2022) 058101, http://dx.doi.org/10.1088/0256-307X/39/5/058101, URL http://cpl.iphy.ac.cn/EN/abstract/article_116110.shtml.

[24] S. Das Sarma, H. Pan, Disorder-induced zero-bias peaks in majorana nanowires, Phys. Rev. B 103 (2021) 195158, http://dx.doi.org/10.1103/PhysRevB.103.195158, URL https://link.aps.org/doi/10.1103/PhysRevB.103.195158.

[25] D.A. Bagrets, Y.V. Nazarov, Full counting statistics of charge transfer in Coulomb blockade systems, Phys. Rev. B 67 (2003) 085316, http://dx.doi.org/10.1103/PhysRevB.67.085316, URL https://link.aps.org/doi/10.1103/PhysRevB.67.085316.

[26] V.F. Maisi, D. Kambly, C. Flindt, J.P. Pekola, Full counting statistics of andreev tunneling, Phys. Rev. Lett. 112 (2014) 036801, http://dx.doi.org/10.1103/PhysRevLett.112.036801, URL https://link.aps.org/doi/10.1103/PhysRevLett.112.036801.

[27] M. Albert, C. Flindt, M. Büttiker, Distributions of waiting times of dynamic single-electron emitters, Phys. Rev. Lett. 107 (2011) 086805, http://dx.doi.org/10.1103/PhysRevLett.107.086805, URL https://link.aps.org/doi/10.1103/PhysRevLett.107.086805.

[28] K. Ptaszyński, Waiting time distribution revealing the internal spin dynamics in a double quantum dot, Phys. Rev. B 96 (2017) 035409, http://dx.doi.org/10.1103/PhysRevB.96.035409, URL https://link.aps.org/doi/10.1103/PhysRevB.96.035409.

[29] K.H. Thomas, C. Flindt, Electron waiting times in non-Markovian quantum transport, Phys. Rev. B 87 (2013) 121405, http://dx.doi.org/10.1103/PhysRevB.87.121405, URL https://link.aps.org/doi/10.1103/PhysRevB.87.121405.

[30] G.-M. Tang, F. Xu, J. Wang, Waiting time distribution of quantum electronic transport in the transient regime, Phys. Rev. B 89 (2014) 205310, http://dx.doi.org/10.1103/PhysRevB.89.205310, URL https://link.aps.org/doi/10.1103/PhysRevB.89.205310.

[31] R. Seoane Souto, R. Avriller, R.C. Monreal, A. Martín-Rodero, A. Levy Yeyati, Transient dynamics and waiting time distribution of molecular junctions in the polaronic regime, Phys. Rev. B 92 (2015) 125435, http://dx.doi.org/10.1103/PhysRevB.92.125435, URL https://link.aps.org/doi/10.1103/PhysRevB.92.125435.

[32] G. Tang, F. Xu, S. Mi, J. Wang, Spin-resolved electron waiting times in a quantum-dot spin valve, Phys. Rev. B 97 (2018) 165407, http://dx.doi.org/10.1103/PhysRevB.97.165407, URL https://link.aps.org/doi/10.1103/PhysRevB.97.165407.

[33] S.L. Rudge, D.S. Kosov, Nonrenewal statistics in quantum transport from the perspective of first-passage and waiting time distributions, Phys. Rev. B 99 (2019) 115426, http://dx.doi.org/10.1103/PhysRevB.99.115426, URL https://link.aps.org/doi/10.1103/PhysRevB.99.115426.

[34] S. Gustavsson, R. Leturcq, M. Studer, I. Shorubalko, T. Ihn, K. Ensslin, D. Driscoll, A. Gossard, Electron counting in quantum dots, Surf. Sci. Rep. 64 (6) (2009) 191–232, http://dx.doi.org/10.1016/j.surfrep.2009.02.001, URL https://www.sciencedirect.com/science/article/pii/S0167572909000193.

[35] M. Jenei, E. Potanina, R. Zhao, K.Y. Tan, A. Rossi, T. Tanttu, K.W. Chan, V. Sevriuk, M. Möttönen, A. Dzurak, Waiting time distributions in a two-level fluctuator coupled to a superconducting charge detector, Phys. Rev. Res. 1 (2019) 033163, http://dx.doi.org/10.1103/PhysRevResearch.1.033163, URL https://link.aps.org/doi/10.1103/PhysRevResearch.1.033163.

[36] F. Brange, A. Schmidt, J.C. Bayer, T. Wagner, C. Flindt, R.J. Haug, Controlled emission time statistics of a dynamic single-electron transistor, Sci. Adv. 7 (2) (2021) eabe0793, http://dx.doi.org/10.1126/sciadv.abe0793.

[37] A. Ranni, F. Brange, E.T. Mannila, C. Flindt, V.F. Maisi, Real-time observation of cooper pair splitting showing strong non-local correlations, Nature Commun. 12 (2021) 6358, http://dx.doi.org/10.1038/s41467-021-26627-8.

[38] D.E. Liu, H.U. Baranger, Detecting a majorana-fermion zero mode using a quantum dot, Phys. Rev. B 84 (2011) 201308, http://dx.doi.org/10.1103/PhysRevB.84.201308, URL https://link.aps.org/doi/10.1103/PhysRevB.84.201308.

[39] H.-F. Lü, H.-Z. Lu, S.-Q. Shen, Enhanced current noise correlations in a Coulomb-majorana device, Phys. Rev. B 93 (2016) 245418, http://dx.doi.org/10.1103/PhysRevB.93.245418, URL https://link.aps.org/doi/10.1103/PhysRevB.93.245418.

[40] M. Aslam, X. feng Chen, Y.-X. Li, Transport properties in quantum dot-majorana bound state structure with ferromagnetic and superconductor leads, Physica E 117 (2020) 113822, http://dx.doi.org/10.1016/j.physe.2019.113822, URL https://www.sciencedirect.com/science/article/pii/S1386947719314213.

[41] H.-F. Lü, H.-Z. Lu, S.-Q. Shen, Nonlocal noise cross correlation mediated by entangled majorana fermions, Phys. Rev. B 86 (2012) 075318, http://dx.doi.org/10.1103/PhysRevB.86.075318, URL https://link.aps.org/doi/10.1103/PhysRevB.86.075318.

[42] H.-F. Lü, H.-Z. Lu, S.-Q. Shen, Current noise cross correlation mediated by majorana bound states, Phys. Rev. B 90 (2014) 195404, http://dx.doi.org/10.1103/PhysRevB.90.195404, URL https://link.aps.org/doi/10.1103/PhysRevB.90.195404.

[43] L. Rajabi, C. Pöltl, M. Governale, Waiting time distributions for the transport through a quantum-dot tunnel coupled to one normal and one superconducting lead, Phys. Rev. Lett. 111 (2013) 067002, http://dx.doi.org/10.1103/PhysRevLett.111.067002, URL https://link.aps.org/doi/10.1103/PhysRevLett.111.067002.

[44] G.T. Landi, Waiting time statistics in boundary-driven free fermion chains, Phys. Rev. B 104 (2021) 195408, http://dx.doi.org/10.1103/PhysRevB.104.195408, URL https://link.aps.org/doi/10.1103/PhysRevB.104.195408.

[45] T. Brandes, Waiting times and noise in single particle transport, Ann. Der Phys. 17 (7) (2010) 477–496, http://dx.doi.org/10.1002/andp.200810306, URL https://onlinelibrary.wiley.com/doi/10.1002/andp.200810306.

[46] C. Emary, C. Pöltl, A. Carmele, J. Kabuss, A. Knorr, T. Brandes, Bunching and antibunching in electronic transport, Phys. Rev. B 85 (2012) 165417, http://dx.doi.org/10.1103/PhysRevB.85.165417, URL https://link.aps.org/doi/10.1103/PhysRevB.85.165417.

[47] N. Walldorf, F. Brange, C. Padurariu, C. Flindt, Noise and full counting statistics of a cooper pair splitter, Phys. Rev. B 101 (2020) 205422, http://dx.doi.org/10.1103/PhysRevB.101.205422, URL https://link.aps.org/doi/10.1103/PhysRevB.101.205422.

[48] S.L. Rudge, D.S. Kosov, Counting quantum jumps: A summary and comparison of fixed-time and fluctuating-time statistics in electron transport, J. Chem. Phys. 151 (3) (2019) 034107, http://dx.doi.org/10.1063/1.5108518.

[49] J. Liu, M.-Q. Shi, Z. Chen, S.-M. Wang, Z.-L. Wang, S.-N. Zhu, Quantum photonics based on metasurfaces, Opto-Electron. Adv. 4 (9) (2021) 200092, http://dx.doi.org/10.29026/oea.2021.200092, URL https://www.oejournal.org/article/doi/10.29026/oea.2021.200092.

[50] Z.-W. Li, W. Yang, M. Huang, X. Yang, C.-G. Zhu, C.-L. He, L.-H. Li, Y.-J. Wang, Y.-F. Xie, Z.-R. Luo, D.-L. Liang, J.-H. Huang, X.-L. Zhu, X.-J. Zhuang, D. Li, A.-L. Pan, Light-triggered interfacial charge transfer and enhanced photodetection in CdSe/Zns quantum dots/MoS2 mixed-dimensional phototransistors, Opto-Electron. Adv. 4 (9) (2021) 210017, http://dx.doi.org/10.29026/oea.2021.210017, URL https://www.oejournal.org/article/doi/10.29026/oea.2021.210017.

[51] C. Cai, S.-B. Han, X.-T. Zhang, J.-X. Yu, X. Xiang, J. Yang, L. Qiao, X.-T. Zu, Y.-Z. Chen, S. Li, Ultrahigh oxygen evolution reaction activity in au doped co-based nanosheets, RSC Adv. 12 (2022) 6205–6213, http://dx.doi.org/10.1039/D1RA09094A.

[52] W. Belzig, Full counting statistics of super-Poissonian shot noise in multilevel quantum dots, Phys. Rev. B 71 (2005) 161301, http://dx.doi.org/10.1103/PhysRevB.71.161301, URL https://link.aps.org/doi/10.1103/PhysRevB.71.161301.

[53] E.B. Hansen, J. Danon, K. Flensberg, Probing electron-hole components of subgap states in Coulomb blockaded majorana islands, Phys. Rev. B 97 (2018) 041411, http://dx.doi.org/10.1103/PhysRevB.97.041411, URL https://link.aps.org/doi/10.1103/PhysRevB.97.041411.

[54] P. Stegmann, B. Sothmann, J. König, C. Flindt, Electron waiting times in a strongly interacting quantum dot: Interaction effects and higher-order tunneling processes, Phys. Rev. Lett. 127 (2021) 096803, http://dx.doi.org/10.1103/PhysRevLett.127.096803, URL https://link.aps.org/doi/10.1103/PhysRevLett.127.096803.